View Article Online / Journal Homepage / Table of Contents for this issue

Organic & Biomolecular Chemistry

Dynamic Article Links

Cite this: *Org. Biomol. Chem.*, 2011, **9**, 2840

www.rsc.org/obc

PAPER

Incorporation of porphyrin acetylides into duplexes of the simplified nucleic acid GNA†

Hui Zhou,[a] Andrew T. Johnson,[b] Olaf Wiest[b] and Lilu Zhang*[a]

Received 16th July 2010, Accepted 24th January 2011
DOI: 10.1039/c0ob00439a

Published on 02 March 2011 on http://pubs.rsc.org | doi:10.1039/C0OB00439A
Downloaded by Brown University on 05 January 2013

A porphyrin-acetylide-modified GNA (glycol nucleic acid) phosphoramidite building block was synthesized in an economical fashion starting from (*S*)-glycidyl-4,4′- dimethoxytrityl ether in just 4 steps with an overall yield of 48%. The porphyrin acetylide nucleotide was incorporated into GNA duplexes opposite ethylene glycol abasic sites and the duplexes were analyzed by UV-melting, UV-vis, fluorescence spectroscopy, and circular dichroism. The modified GNA duplexes display lower thermal stabilities, however, the stabilities of the duplexes can be modulated by the incorporation of Zn^{2+} (further destabilization) or Ni^{2+} (stabilization relative to the uncomplexed porphyrin). Uncomplexed as well as Ni^{2+}-coordinated porphyrins intercalate into the GNA duplex whereas Zn^{2+}-coordinated porphyrins are most likely located outside the base stack. Adjacent porphyrins in opposite strands of GNA duplexes show an electronic interaction with each other which might be exploited in the future for the design of photoelectrical devices.

Introduction

Chromophores play important roles as imaging tools in the life sciences, as components for industrial dyes and pigments, and in natural processes such as photosynthesis. The conversion of sunlight into chemical energy by photosystems I and II relies on a controlled and defined arrangement of the chlorphyll chromophores for providing efficient light absorption, energy transfer, and the initiation of charge separation. This example reveals that the function of chromophore arrays relies on a controlled spatial organization of the individual chromophores and it is therefore not surprising that the design of defined chromophore arrays is receiving an increasing interest.[1–4]

DNA is currently extensively used as a scaffold for the self-assembly of structures with defined positioning of multiple chromophores and other functional moieties.[5–7] In this respect, DNA offers two key advantages: (1) The canonical Watson–Crick base pairing scheme allows the construction of defined helical architectures with high predictability. (2) Highly reliable automated oligonucleotide synthesis enables the solid-phase synthesis of oligonucleotides bearing multiple site-specific modifications.

Porphyrins have been widely investigated due to their unique photochemical and photophysical properties. Defined multi-porphyrin arrays are attractive for the design of artificial light harvesting systems and photoelectrical devices.[8] With this or related purposes in mind, DNA has been used as supramolecular scaffold to arrange porphyrins in a controlled fashion. Porphyrins have been covalently attached to nucleobases,[9–10] the deoxyribose moiety,[11] and internal phosphorus atoms of DNA strands.[12] A recent report dealt with the attachment of porphyrins to deoxyuridine *via* a rigid acetylene spacer for exploring the use of DNA as a scaffold to create helical multiporphyrin arrays.[9] However, interestingly, there are only very few reports in which porphyrins are placed in the interior of the DNA as part of the π-stacking, most likely due to the challenging synthesis of the necessary porphyrin nucleotide building blocks.[13]

We recently initiated a research program that aims to use the simplified nucleic acid GNA (glycol nucleic acid) as a convenient duplex scaffold for the generation of functional architectures.[14] GNA is composed of nucleobases attached to propane-1,2-diol as nucleoside building blocks that are connected by phosphodiester bonds (Fig. 1a). GNA duplexes combine high duplex stability and base pairing fidelity with a structurally simplified acyclic backbone.[15–17] X-ray crystal structures of (*S*)-GNA duplexes reveal that the overall GNA double helix is distinguished from canonical A- and B-form nucleic acids and might be best described as a helical ribbon loosely wrapped around the helix axis.[16,18] (*S*)-GNA undergoes extensive zipper-like interstrand interactions and at the same time possesses a reduced intrastrand base–base stacking interaction due to a large average slide between neighboring base

[a]*Fachbereich Chemie, Philipps-Universität Marburg, Hans-Meerwein-Straße, D-35032, Marburg, Germany. E-mail: zhangl@staff.uni-marburg.de; Fax: +49-6421-2822189; Tel: +49-6421-2825600*
[b]*Department of Chemistry and Biochemistry, University of Notre Dame, Notre Dame, Indiana, 46556-5670, USA*

† Electronic supplementary information (ESI) available: Absorption spectra of GNA single strands with and without metals; UV-vis spectra of GNA duplexes and their corresponding single strands; concentration-dependent and salt concentration-dependent UV-vis spectra of single strands **ON10**, **ON11** and their duplex **ON10**:**ON11**; temperature-dependent UV-vis spectra of duplexes at Soret band region; fluorescence spectra of **ON12**, **ON13** and **ON12**:**ON13**, and $\mathbf{ON12^{Zn}}$, $\mathbf{ON13^{Zn}}$ and $\mathbf{ON12^{Zn}}$:$\mathbf{ON13^{Zn}}$; Maldi-TOF data of all oligonucleotides. See DOI: 10.1039/c0ob00439a

This journal is © The Royal Society of Chemistry 2011

Published on 02 March 2011 on http://pubs.rsc.org | doi:10.1039/C0OB00439A
Downloaded by Brown University on 05 January 2013

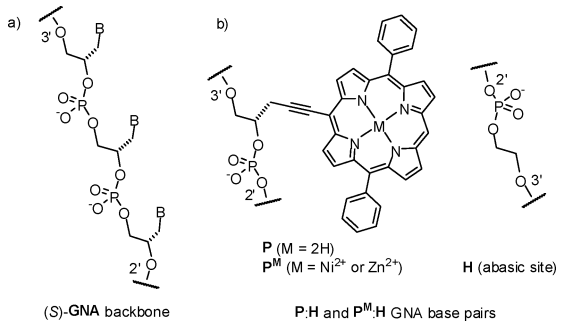

Fig. 1 (a) Constitution of the (*S*)-GNA backbone;(b) **P**:**H** and **P**^{M}:**H** base pairs used in this study.

pairs. Furthermore, (*S*)-GNA only displays one large groove, whereas the canonical major groove is a convex surface. This different duplex architecture might offer new opportunities to arrange functional molecules such as chromophores in a controlled and unique fashion. Thus, high duplex stabilities exceeding the stabilities of analogous DNA and RNA duplexes, in combination with an economical and fast synthesis of (modified) phosphoramidite building blocks render GNA an attractive nucleic acid scaffold for biotechnology and nanotechnology.

Here we report the first synthesis of a porphyrin-modified GNA nucleotide, its incorporation into GNA, and the behavior of such non-metallated and metallated porphyrins in the context of GNA duplexes.

Results and Discussions

Synthesis of a porphyrin acetylide GNA nucleotide and its incorporation into GNA oligonucleotides

We were seeking a propane-1,2-diol-modified porphyrin building block that (a) is capable of stacking in GNA duplexes opposite an ethylene glycol spacer as shown in Fig. 1b and (b) is at the same time synthetically easily accessible. Based on these two criteria we selected the phosphoramidite building block **1** as our target. Accordingly, (*S*)-glycidyl-4,4′-dimethoxytrityl ether **2** was reacted with trimethylsilyl (TMS) acetylene in the presence of *n*-BuLi and boron trifluoride etherate to produce in a regioselective and stereospecific epoxide ring opening the acetylenic alcohol **3** in 70% yield. After removal of the TMS group of **3** with TBAF (98%), a Pd-catalyzed Sonogashira coupling with 5-bromo-10,20-diphenylporphinatozinc **5** afforded **6** smoothly in 95% yield. Further reaction with 2-cyanoethyl-*N*,*N*-diisopropylchlorophosphoramidite in the presence of Hünig's base yielded the phosphoramidite building block **1** (74%). Thus, phosphoramidite **1** was synthesized in a straightforward fashion starting from epoxide **2** in just four steps with an overall yield of 48% (Scheme 1).

Next, phosphoramidite **1** was used to synthesize GNA strands with incorporated diphenylporphyrin acetylide nucleotides (**P**, Fig. 1b). GNA oligonucleotides were synthesized on CPG supports with standard protocols for 2-cyanoethylphosphoramidites. Due to its low solubility in the standard solvent acetonitrile, phosphoramidite **1** was dissolved in THF for the use in the DNA synthesizer and the coupling times were extended to 15 min. The GNA strands were synthesized in trityl-on mode and cleaved from the resin with concentrated ammonia at 55 °C for 12 h. After cooling to room temperature, the entire solution of crude tritylated oligonucleotides was applied directly to a Sep–Pak classic reversed-phase column and subsequently washed, detritylated with 1.5% aqueous TFA, and then eluted from the column using 30% aqueous acetonitrile. After an additional purification step with a reversed phase HPLC column, the porphyrin-containing GNA strands were obtained in high purities and devoid of the zinc ions, most likely due to the acidic conditions during the individual detritylation steps. However, zinc and nickel ions could be readily (re)introduced into the coordination sites of the porphyrin nucleotides in GNA oligunucleotides to give **P**^{M} (Fig. 1b) by mixing the purified single strands with $Zn(OAc)_2$ or $Ni(OAc)_2$ in Tris-HCl buffered solution.

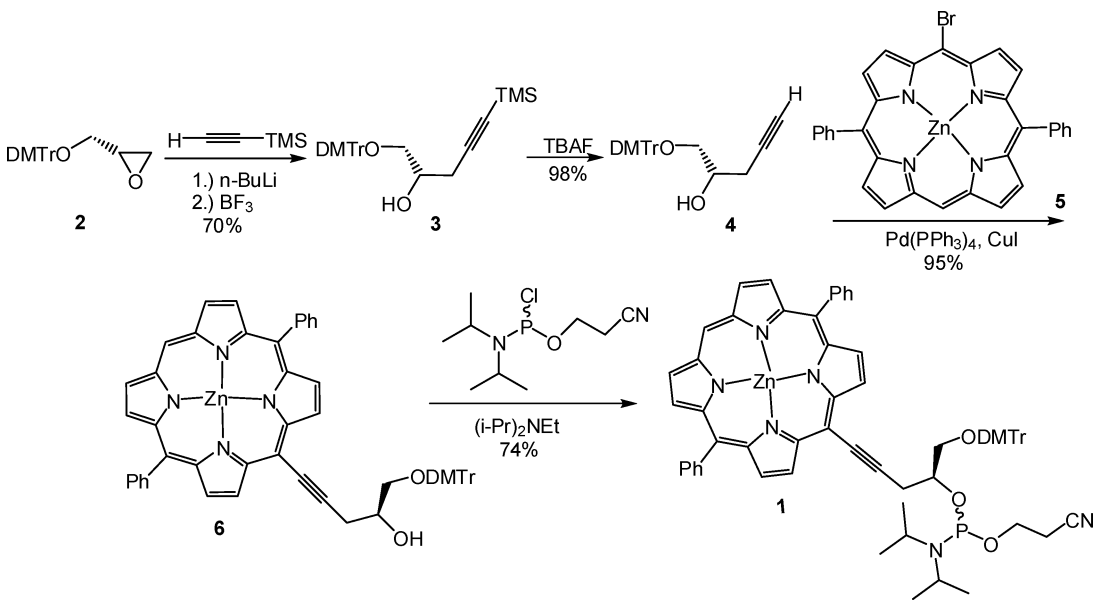

Scheme 1 Synthesis of the porphyrin acetylide phosphoramidite **1**.

Published on 02 March 2011 on http://pubs.rsc.org | doi:10.1039/C0OB00439A
Downloaded by Brown University on 05 January 2013

Investigation of duplex stabilities

We first investigated the stability of GNA duplexes containing a single non-metallated (**P**) or metallated porphyrin ($\mathbf{P^M}$). Table 1 shows the UV-melting data of duplexes with **P** and $\mathbf{P^M}$ incorporated into the position 8 of 16mer duplexes and two reference duplexes. It is noteworthy that all GNA duplexes investigated in this work do only contain A and T nucleotides in order to keep the GNA scaffold as simple as possible. Pairing **P** with the ethylene glycol abasic site **H** afforded a duplex melting point (T_m) of 48 °C (Table 1, entry 3), compared to 54 °C for an A:T base pair at the same position (Table 1, entry 1). Removing one A:T base pair of the Watson–Crick reference duplex as in **ON3**:**ON4** (Table 1, entry 2) resulted in a melting point of 52 °C, thus demonstrating that the incorporation of a single **P**:**H** base pair has a net destabilizing effect of $\Delta T_m = 4$ °C. Replacing the abasic site **H** of the **P**:**H** base pair in **ON6**:**ON7** (Table 1, entry 3) for the natural nucleobases T or A, resulting in **P**:T and **P**:A base pairs, reduces the stability by additional 4 and 3 °C, respectively (Table 1, entries 4 and 5). Apparently, these larger natural nucleobases cannot be accommodated well opposite the space consuming diphenylporphyrin acetylide nucleobase **P**, suggesting that the porphyrin nucleobase is accommodated within the π-stacking of the GNA duplex. Interestingly, the incorporation of a Zn^{2+} ion in the porphyrin results in a significant further destabilization for the $\mathbf{P^{Zn}}$:**H** base pair (T_m = 42 °C, Table 1, entry 6), whereas the incorporation of a Ni^{2+} ion slightly increases the stability compare to **P**:**H** (ΔT_m = + 1 °C), and is only by 3 °C less stable than **ON3**:**ON4**. These modulations of duplex stabilities by the nature of the metal ion incorporated into the porphyrin nucleobases can be interpreted by their different coordination behavior. Zn^{2+} prefers to coordinate to axial ligands when incorporated into a porphyrin in an octahedral fashion and needs to dissociate these ligands if it wants to stack within GNA between neighboring base pairs. In contrast, Ni^{2+} prefers square planar coordination and can therefore be accommodated easily in the base stacking.[19]

We also investigated duplexes that contain two adjacent porphyrin acetylide base pairs. Incorporation of a second adjacent **P**:**H** base pair positioning the porphyrins on opposite strands (Table 1, entry 9) reduces the duplex melting temperature further (T_m = 43 °C), being 6 °C below the melting temperatue of a reference Watson–Crick duplex that is devoid of the two **P**:**H** base pairs (Table 1 entry 8). Nevertheless the incorporation of two adjacent **P**:**H** base pairs still affords a duplex that is thermally stable at room temperature. As expected, the introduction of Zn^{2+} ions into the two porphyrins strongly destabilized the duplex to T_m = 34 °C (Table 1, entry 10), similar to what was observed with a single Zn^{2+} porphyrin in GNA (Table 1, entry 6).

Because of this general destabilization trend, we continued to evaluate duplexes containing two porphyrins in longer (22mer) and thus more stable duplexes as displayed in Table 2. These data confirm that two adjacent **P**:**H** base pairs in opposite orientation lead to a destabilization relative to a reference duplex **ON12**:**ON13** and **ON14**:**ON15** containing only A:T base pairs but still provide duplexes with robust stabilities (Table 2, entries 1–4) and this stability can be modulated by the incorporation of Zn^{2+} (further destabilization) and Ni^{2+} (stabilization relative to the free porphyrin) with the nickel(II) containing duplex $\mathbf{ON16^{Ni}}$:$\mathbf{ON17^{Ni}}$ being only by 1 °C less stable compared to the reference duplex (Table 2, entries 5–10).

It is noteworthy that the slopes of the melting curves of GNA duplexes containing porphyrins are more shallow compared to the related unmodified duplexes which might be caused by lower cooperativity among the nucleobases owing to interference by the porphyrin macrocycle (Fig. 2). In addition, the hyperchromicity of the GNA duplexes containing porphyrins is reduced, presumably due to a weaker stacking of base pairs in proximity of **P**:**H** base pairs.

Table 1 Thermal stabilities of porphyrin-containing 16mer GNA duplexes together with Watson–Crick reference duplexes[a]

Entry	Sequence	T_m (°C)
1	3′-TAAAAATAATAATATT-2′ (**ON1**) 2′-ATTTTTATTATTATAA-3′ (**ON2**)	54
2	3′-TAAAAATATAATATT-2′ (**ON3**) 2′-ATTTTTATATTATAA-3′ (**ON4**)	52
3	3′-TAAAAAT**P**ATAATATT-2′ (**ON6**) 2′-ATTTTTA**H**TATTATAA-3′ (**ON7**)	48
4	3′-TAAAAAT**P**ATAATATT-2′ (**ON6**) 2′-ATTTTTA**T**TATTATAA-3′ (**ON2**)	44
5	3′-TAAAAAT**P**ATAATATT-2′ (**ON6**) 2′-ATTTTTAATATTATAA-3′ (**ON5**)	45
6	3′-TAAAAAT$\mathbf{P^{Zn}}$ATAATATT-2′ ($\mathbf{ON6^{Zn}}$) 2′-ATTTTTA**H**TATTATAA-3′ (**ON7**)	42
7	3′-TAAAAAT$\mathbf{P^{Ni}}$ATAATATT-2′ ($\mathbf{ON6^{Ni}}$) 2′-ATTTTTA**H**TATTATAA-3′ (**ON7**)	49
8	3′-TAAAAATTAATATT-2′ (**ON8**) 2′-ATTTTTAATTATAA-3′ (**ON9**)	49
9	3′-TAAAAAT**PH**TAATATT-2′ (**ON10**) 2′-ATTTTTA**HP**ATTATAA-3′ (**ON11**)	43
10	3′-TAAAAAT$\mathbf{P^{Zn}}$**H**TAATATT-2′ ($\mathbf{ON10^{Zn}}$) 2′-ATTTTTA**HP**$\mathbf{^{Zn}}$ATTATAA-3′ ($\mathbf{ON11^{Zn}}$)	34

[a] Conditions: 10 mM sodium phosphate, 100 mM NaCl, and 2 μM individual strands.

Table 2 Thermal stabilities of porphyrin-containing 22mer GNA duplexes and Watson–Crick reference duplexes[a]

Entry	Sequence	T_m (°C)
1	3′-TTATAAAAATAATAATATTAAT-2′ (**ON12**) 2′-AATATTTTTATTATTATAATTA-3′(**ON13**)	63
2	3′-TTATAAAAATTAATATTAAT-2′ (**ON14**) 2′-AATATTTTTAATTATAATTA-3′(**ON15**)	61
3	3′-TTATAAAAAT**PH**TAATATTAAT-2′ (**ON16**) 2′-AATATTTTTA**HP**ATTATAATTA-3′(**ON17**)	56
4	3′-TTATAAAAAT**HP**TAATATTAAT-2′ (**ON18**) 2′-AATATTTTTA**PH**ATTATAATTA-3′(**ON19**)	56
5	3′-TTATAAAAAT$\mathbf{P^{Zn}}$**H**TAATATTAAT-2′ ($\mathbf{ON16^{Zn}}$) 2′-AATATTTTTA**HP**$\mathbf{^{Zn}}$ATTATAATTA-3′($\mathbf{ON17^{Zn}}$)	48
6	3′-TTATAAAAAT$\mathbf{P^{Ni}}$**H**TAATATTAAT-2′ ($\mathbf{ON16^{Ni}}$) 2′-AATATTTTTA**HP**$\mathbf{^{Ni}}$ATTATAATTA-3′($\mathbf{ON17^{Ni}}$)	59
7	3′-TTATAAAAAT**HP**$\mathbf{^{Zn}}$TAATATTAAT-2′ ($\mathbf{ON18^{Zn}}$) 2′-AATATTTTTA$\mathbf{P^{Zn}}$**H**ATTATAATTA-3′($\mathbf{ON19^{Zn}}$)	49
8	3′-TTATAAAAAT**HP**$\mathbf{^{Ni}}$TAATATTAAT-2′ ($\mathbf{ON18^{Ni}}$) 2′-AATATTTTTA$\mathbf{P^{Ni}}$**H**ATTATAATTA-3′($\mathbf{ON19^{Ni}}$)	60
9	3′-TTATAAAAAT$\mathbf{P^{Zn}}$**H**TAATATTAAT-2′ ($\mathbf{ON16^{Zn}}$) 2′-AATATTTTTA**HP**$\mathbf{^{Ni}}$ATTATAATTA-3′($\mathbf{ON17^{Ni}}$)	54
10	3′-TTATAAAAAT$\mathbf{P^{Ni}}$**H**TAATATTAAT-2′ ($\mathbf{ON16^{Ni}}$) 2′-AATATTTTTA**HP**$\mathbf{^{Zn}}$ATTATAATTA-3′($\mathbf{ON17^{Zn}}$)	52

[a] Conditions: 10 mM sodium phosphate, 100 mM NaCl, and 2 μM individual strands.

This journal is © The Royal Society of Chemistry 2011

Published on 02 March 2011 on http://pubs.rsc.org | doi:10.1039/C0OB00439A
Downloaded by Brown University on 05 January 2013

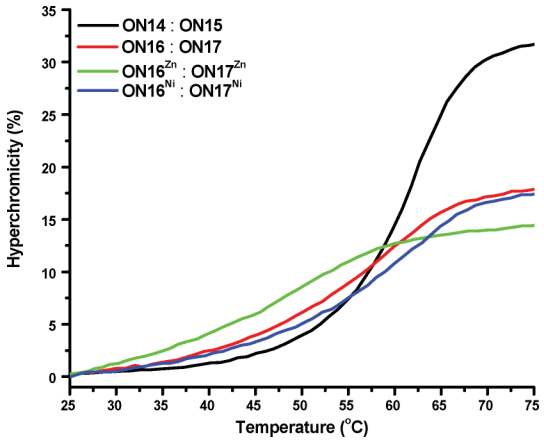

Fig. 2 UV-melting curves of duplexes **ON14**:**ON15**, **ON16**:**ON17**, **ON16^{Zn}**:**ON17^{Zn}** and **ON16^{Ni}**:**ON17^{Ni}** (see Table 2 for the sequences). Changes in absorbance upon heating as monitored at 260 nm. Conditions: 10 mM sodium phosphate, 100 mM NaCl, pH 7.0, and 2 μM of each strand.

UV-vis spectroscopy

Due to increased duplex stabilities we investigated the UV-vis absorption properties of porphyrin GNA strands and the corresponding duplexes with the 22mer system (Table 2). We began by analyzing porphyrin-modified single strands without and with incorporated zinc(II) and nickel(II) ions. The UV-vis spectra of the single strands **ON16**, **ON16^{Zn}**, and **ON16^{Ni}** are shown in Fig. 3 and clearly confirm the successful insertion of the metal ions into the porphyrins. The absorption spectrum of **ON16** displays a Soret band at 426 nm and four Q bands, while **ON16^{Zn}** and **ON16^{Ni}** exhibit one Soret band at 430 nm and 421 nm, respectively, and just two Q bands. The reduced number of Q bands is typical of metalloporphyrins.[20] In addition, the observed slight red shift of the Soret band for **ON16^{Zn}** and blue shift for **ON16^{Ni}** are consistent with the well-known red shift of porphyrin Soret bands upon Zn(II) coordination, and blue shift of Soret bands upon Ni(II) coordination.[20] UV-vis spectra of single strands **ON17**, **ON18**, **ON19** and their metal derivatives are provided in the supporting information.

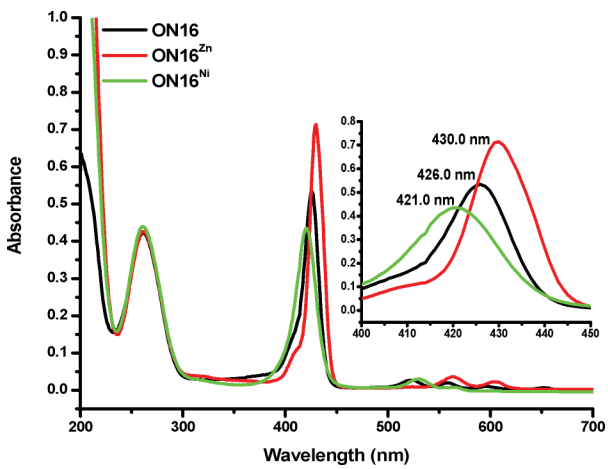

Fig. 3 Absorption spectra of **ON16**, **ON16^{Zn}** and **ON16^{Ni}**. The insert shows the expanded porphyrin Soret band region. Conditions: 10 mM sodium phosphate, 100 mM NaCl, pH 7.0, and 2 μM of single strands.

We next compared the UV-vis spectra of duplexes and their corresponding single strands in order to obtain information about the relative orientations of the porphyrin units in the GNA duplexes. Pronounced changes in the absorption spectra were observed upon duplex formation as displayed in Fig. 4 and Fig. S2.† Duplex **ON16**:**ON17**, **ON16^{Zn}**:**ON17^{Zn}** and **ON16^{Zn}**:**ON17^{Ni}** show a clear peak split of the Soret band. The splitting energies between the low- and high-energy Soret bands are 920 cm^{-1} for duplex **ON16**:**ON17**, 962 cm^{-1} for duplex **ON16^{Zn}**:**ON17^{Zn}** and with the mixed metal porphyrin duplex **ON16^{Zn}**:**ON17^{Ni}** having the highest excition energy (1151 cm^{-1}). The duplex **ON16^{Ni}**:**ON17^{Ni}** exhibits a broadened Soret band instead of two distinct peaks. An obvious change of the Soret bands of the duplex accompanied by a blue shift indicates a ground-state interaction of the two porphyrin moieties. It has been reported that split Soret bands can be caused by dipole–dipole exciton coupling from slipped-cofacial interactions between two porphyrins.[21] Thus, the two neighboring porphyrin units in the GNA duplex might adopt a slipped-cofacial geometry. The Soret band of all duplexes shift

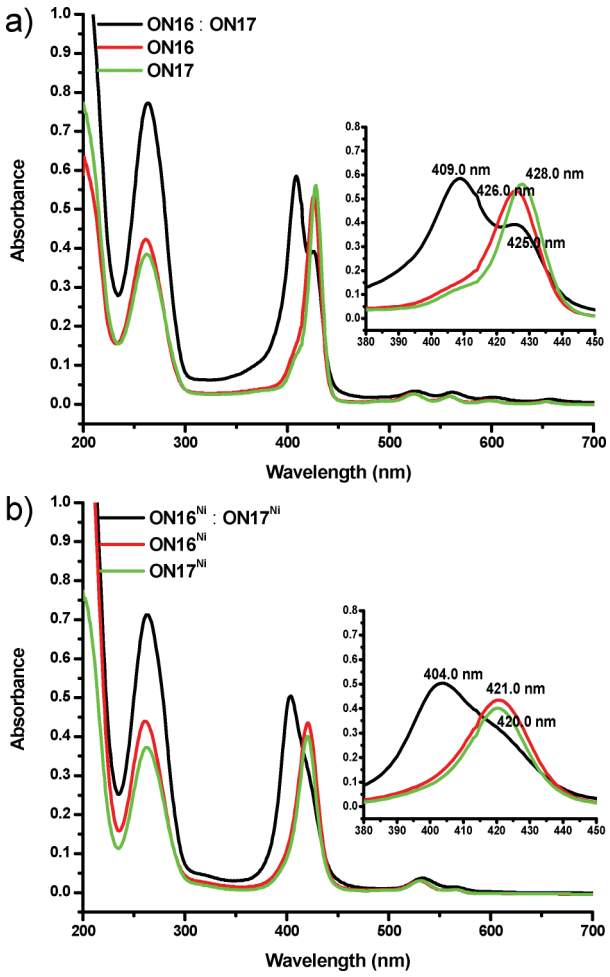

Fig. 4 UV-vis spectra of GNA duplexes and their corresponding single strands. (a) **ON16**, **ON17** and **ON16**:**ON17**; (b) **ON16^{Ni}**, **ON17^{Ni}** and **ON16^{Ni}**:**ON17^{Ni}** The inserts show expanded porphyrin Soret band regions. Conditions: 10 mM sodium phosphate, 100 mM NaCl, pH 7.0, and 2 μM of each strand.

Published on 02 March 2011 on http://pubs.rsc.org | doi:10.1039/C0OB00439A
Downloaded by Brown University on 05 January 2013

to a shorter wavelengths, indicating that in each duplex two porphyrin units overlap face-to-face (H-dimer).[22]‡

Next, we measured the influence of temperature on the UV-vis spectra for the duplexes **ON16**:**ON17**, **ON16**^{Zn}:**ON17**^{Zn}, **ON16**^{Ni}:**ON17**^{Ni} and **ON16**^{Zn}:**ON17**^{Ni}. The results are shown in Fig. 5 and Fig. S5† and reveal strong spectral changes in the Soret band of the porphyrin moieties upon heating from 20 °C to 80 °C. By increasing the temperature, the peaks gradually shift to a longer wavelength with disappearance of the splitting of the peaks and this shift can be associated with a dissociation of the duplexes into their single strands: two porphyrin moieties in two strands lose their interaction.

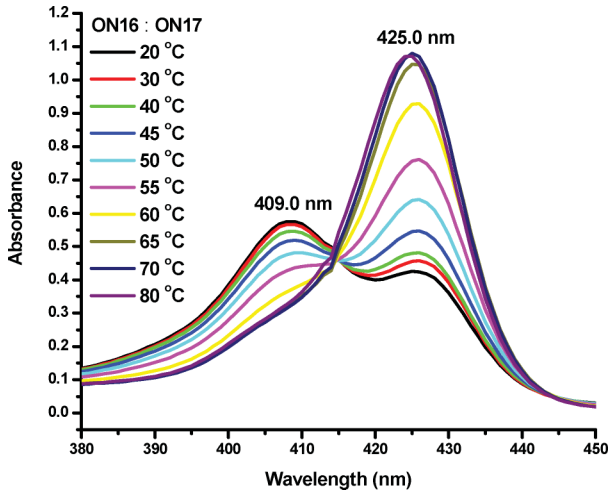

Fig. 5 Temperture-dependent UV-vis spectra of duplexes of **ON16**:**ON17** at the Soret band region. Conditions: 10 mM sodium phosphate, 100 mM NaCl, pH 7.0 and 2 μM of each strand.

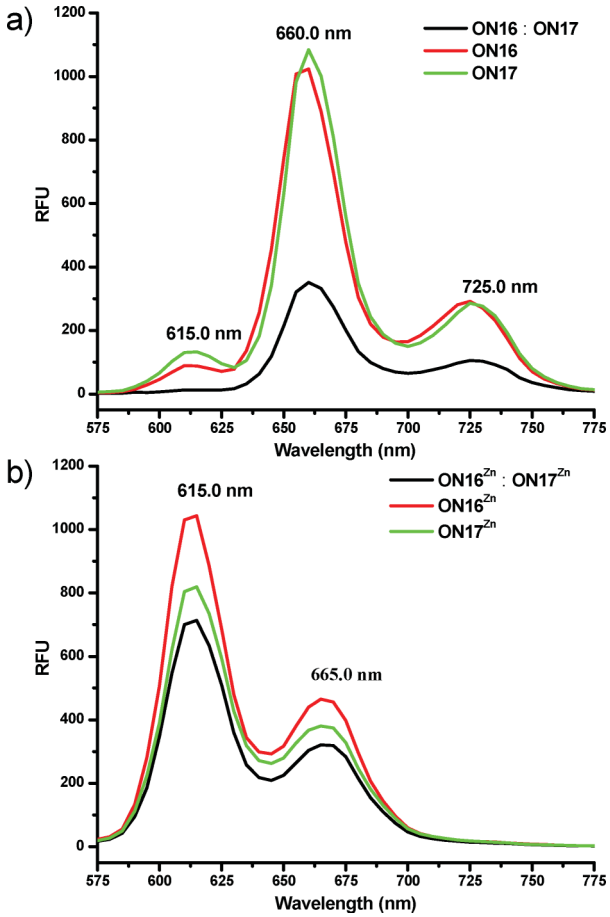

Fig. 6 Fluorescence spectra of GNA duplexes and their corresponding single strands. (a) **ON16**, **ON17** and **ON16**:**ON17**; (b) **ON16**^{Zn}, **ON17**^{Zn} and **ON16**^{Zn}:**ON17**^{Zn}. Conditions: 10 mM sodium phosphate, 100 mM NaCl, pH 7.0 and 2 μM of each strand.

Fluorescence spectroscopy

The fluorescence spectra of **ON16**, **ON17**, **ON16**:**ON17**, and **ON16**^{Zn}, **ON17**^{Zn}, **ON16**^{Zn}:**ON17**^{Zn} are shown in Fig. 6. Ni porphyrins could not be investigated since they are not fluorescence.[18] **ON16** and **ON17** which contain free porphyrins display the characteristic two emission peaks at 660 nm and 725 nm, while **ON16**^{Zn} and **ON17**^{Zn} show features of Zn prophyrin emission spectra: the emission peaks are situated at 615 nm and 665 nm which are 50 nm blue shifted compare to **ON16** and **ON17**.[20] Apart from the change in intensity, the fluorescent spectra of duplexes **ON16**:**ON17** and **ON16**^{Zn}:**ON17**^{Zn} are rather similar. The decrease of fluorescence intensity is consistent with the formation of porphyrin aggregates. In addition, **ON16**:**ON17** shows lower emission quantity compared to **ON16**^{Zn}:**ON17**^{Zn}, which is in agreement with the fact that the free porphyrins can stack better within the GNA duplex. Overall, the UV-vis together with the fluorescence data support interactions between the porphyrins within the GNA duplex.

CD spectroscopy

In order to learn more about the interaction of the porphyrins with the GNA duplex, porphyrin-modified GNA duplexes were investigated by CD spectroscopy as shown in Fig. 7. The CD signals of porphyrin-GNA duplexes in the GNA absorption region are almost identical to those of the native GNA duplex, except for the lower signal intensities. It thus seems that the porphyrin modifications do not distort the overall GNA duplex conformation to a significant extent. In the porphyrin absorption region, induced negative Cotton effects at 406 nm and 400 nm are observed in the case of **ON16**:**ON17** (Fig. 7a) and **ON16**^{Ni}:**ON17**^{Ni} (Fig. 7c). Typically for DNA-porphyrins, an induced negative Cotton effect in the Soret region is a signature of the intercalation of the porphyrin moiety into the DNA duplex.[23,24] Together with the T_m data, we therefore conclude that the porphyrin rings in duplex **ON16**:**ON17** and **ON16**^{Ni}:**ON17**^{Ni} intercalate into the GNA duplex and stack to neighboring base pairs. However, the CD spectra of duplexes which contain Zn-porphyrins are different. In the case of **ON16**^{Zn}:**ON17**^{Zn} (Fig. 7b), a clear multisignate CD spectrum, consisting of two negative bands at 409 and 429 nm and a positive band at 441 nm is observed. The CD spectrum of **ON16**^{Zn}:**ON17**^{Ni} (Fig. 7d) shows a strong negative

‡ Uv-vis spectra of single strands and duplexes are independent of strand and salt concentrations. Concentration and salt-dependent UV-vis spectra are shown in the ESI.†

This journal is © The Royal Society of Chemistry 2011

Published on 02 March 2011 on http://pubs.rsc.org | doi:10.1039/C0OB00439A
Downloaded by Brown University on 05 January 2013

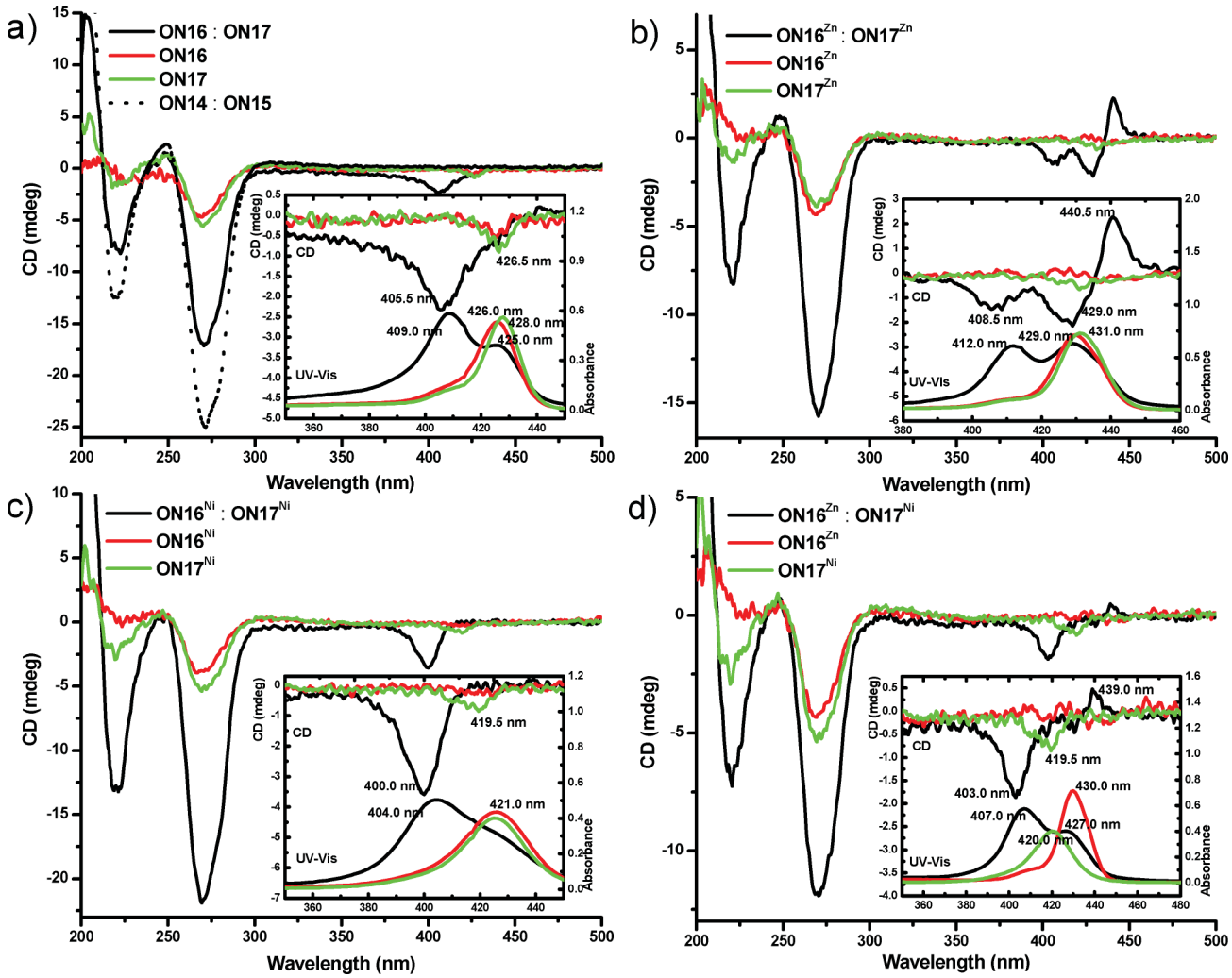

Fig. 7 CD spectra of GNA duplexes and their corresponding single strands. (a) **ON16**, **ON17**, **ON16**:**ON17** and **ON14**:**ON15**; (b) **ON16**^{Zn}, **ON17**^{Zn} and **ON16**^{Zn}:**ON17**^{Zn}; (c) **ON16**^{Ni}, **ON17**^{Ni} and **ON16**^{Ni}:**ON17**^{Ni}; (d) **ON16**^{Zn}, **ON17**^{Ni} and **ON16**^{Zn}:**ON17**^{Ni}. Inserts: Overlap plot of CD and absorption spectra at the Soret region. Conditions: 10 mM sodium phosphate, 100 mM NaCl, pH 7.0, and 12 μM of each strand.

band at 403 nm and a weak positive band at 439 nm. Bisignate or multisignate CD spectra were observed in a system with porphyrins covalently attached to the 5′-end of DNA duplexes and such CD spectra were interpreted for the evidence of through space dipole–dipole electronic interactions between the two porphyrin chromophores.[25] Together with the temperature melting results (Tables 1 and 2), we therefore assume that the Zn-porphyrins interact with each other although they are not as close in contact as the porphyrins in the analogous systems devoid of any metal or coordinated to nickel ions.

Computational work

In order to gain further insight into the binding mode of porphyrin acetylide nucleobases within GNA duplexes, we built models of **ON6**:**ON7** (16mer duplex with single **P**:**H** base pair) and **ON10**:**ON11** (16mer duplex with two adjacent **P**:**H** base pairs) and studied them by molecular dynamics simulations in analogy to our previously described GNA model.[26] Fig. 8 shows the local environment around the porphyrins of the calculated average structures. It is apparent that the porphyrin moieties are well accommodated within the base stacking with only minor distortions of the overall duplex structure and with little or no disruption of hydrogen bonding between the flanking A-T base pairs. For both systems studied, the average interstrand P–P distance for the incorporation sites is 17.0 Å *versus* 16.6 Å for a canonical GNA base pair, with the porphyrin slightly pertruding beyond the band formed by the GNA duplex. Close π-stacking interactions are observed between the porphyrin base and the neighboring base pairs. In **ON10**:**ON11**, the two porphyrins are stacked on top of each other as shown in Fig. 8b. The observed offset of the porphyrins in the calculated structures is in excellent agreement with the experimental observation of the split Soret band seen in the UV-Vis spectra of the related duplex **ON16**:**ON17** (Fig. 4). These slipped cofacial geometries allow the phenyl subsituents of the two adjacent porphyrins to pack efficiently in a face-to-face or edge-to-face fashion, thus explaining the experimental observation that the relative destabilization of two adjacent **P**:**H** base pairs is smaller than a single **P**:**H** base pair within GNA (Table 1, entries 3 and 9).

Published on 02 March 2011 on http://pubs.rsc.org | doi:10.1039/C0OB00439A
Downloaded by Brown University on 05 January 2013

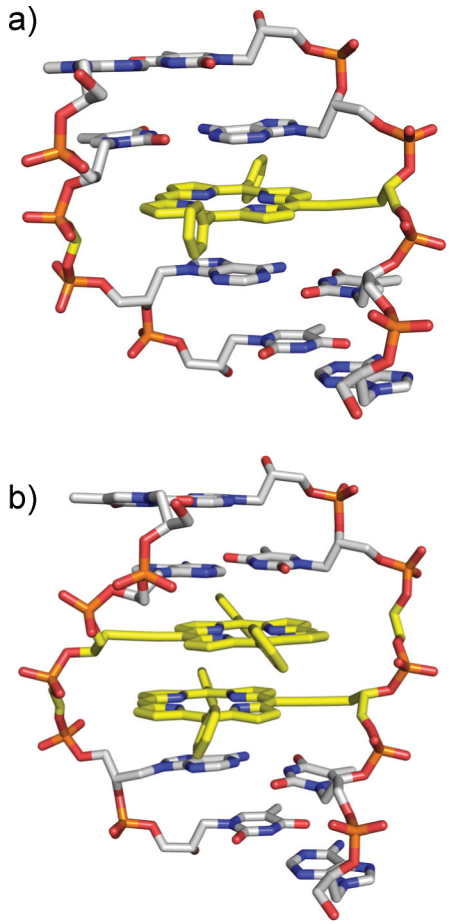

Fig. 8 Calculated structures of the porphyrin-containing duplexes **ON6**:**ON7** (Table 1, entry 3) and **ON10**:**ON11** (Table 2, entry 3). Only the local environment around the **P**:**H** base pairs is shown.

Conclusions

We here reported a straightforward synthetic strategy to employ GNA as a scaffold to organize porphyrin chromophores. A diphenylporphyrin acetylide phosphoramidite GNA building block **1** for automated oligonucleotide synthesis was synthesized in just four steps with an overall yield of 48%. Incorporated opposite an ethylene glycol abasic site (**H**), such porphyrin acetylides (**P**) afford duplexes which are thermally destabilized but without significant perturbation of the overall GNA duplex structures. Interestingly, the thermal stabilities of such **P**:**H** base pairs can be modulated by the incorporation of zinc(II) and nickel(II) which lead to a decrease and increase in duplex stabilities, respectively. This can be rationalized with a flipped-out conformation of the zinc-porphyrin in contrast to a stacking of the nickel-porpyhrin within the base stacking of the GNA duplex. Thus, the conformation of porphyrins in GNA can be modulated by the nature of the coordinated metal ions. Finally, we demonstrated that GNA duplexes are a suitable scaffold for bringing two porphyrins into close contact and to allow the interaction of porphyrins with different coordinated metal ions. Future work will investigate applications of such porphyrin-GNA conjugates and other chromophores for light harvesting and charge transport.

Experimental

Synthesis of porphyrin acetylide phosphoramidite

NMR spectra were recorded on a Brucker AVANCE 300 and Brucker DRX 500. Low-resolution mass spectra were obtained on an LC platform from Agilent using ESI technique. High-resolution mass spectra were obtained on a Thermo Finnigan LTQ FT instrument using APCI ionization. MALDI were obtained on a Ultraflex from Bruker. Infrared spectra were recorded on a Brucker "Alpha-P" FT-IR spectrometer. HPLC was performed using an Agilent technologies 1200 series instrument with fraction collection. All non-aqueous operations were carried out under dry nitrogen atmosphere. Solvents and reagents used as supplied from Aldrich, Alfa Aesar or Acros. 5-Bromo-10, 20-diphenylporphinatozinc **5** was synthesized as reported.[27–29]

Compound 3. To a solution of ethynyltrimethylsilane (0.47 mL, 3.32 mmol) in dry THF (8 mL) at −78 °C was added slowly a 1.6 M hexane solution of *n*-BuLi (2.1 mL, 3.36 mmol). After stirring for 10 min, boron trifluoride diethyl etherate (0.42 mL, 3.32 mmol) was added dropwise. After an additional 5 min at −78 °C, a solution of compound **2**[30] (1.25 g, 3.32 mmol) in anhydrous THF (4 mL) was added slowly. The resulting solution was stirred for 15 min at −78 °C. The reaction was then quenched with saturated aqueous $NaHCO_3$ (80 mL) at −78 °C and extracted with CH_2Cl_2 (3 × 60 mL). The combined organic layers were dried over anhydrous Na_2SO_4, concentrated by rotary evaporation, and purified by flash chromatography over silica gel eluting with hexane–ethyl acetate/triethylamine (10 : 1 : 0.01), affording compound **3** as a colorless oil (1.11 g, 70%). ^{1}H NMR (300 MHz, $CDCl_3$): δ = 7.45 (m, 2H), 7.16–7.38 (m, 7H), 6.84 (d, *J* = 8.9 Hz, 4H), 3.92 (m, 1H), 3.79 (s, 6H), 3.24 (m, 2H), 2.52 (d, *J* = 6.4 Hz, 2H), 0.115 (s, 9H). ^{13}C NMR (75 MHz, $CDCl_3$): δ = 158.65, 144.92, 136.08, 130.18, 128.26, 127.96, 126.95, 113.30, 102.79, 87.34, 86.32, 69.49, 66.10, 55.30, 25.46, 0.14. IR (thin film): 2956, 2933, 2175, 1607, 1580, 1508, 1462, 1445, 1414, 1335, 1298, 1246, 1174, 1155,1075, 1032, 826, 790, 756, 726, 701, 645, 583 cm^{-1}. HRMS: *m*/*z* [M + Na]$^+$ calcd for $C_{29}H_{34}O_4Si_1Na_1$: 497.2119; found: 497.2120.

Compound 4. To a solution of compound **3** (1.73 g, 3.65 mmol) in THF (36.5 mL) was added 1.0 M THF solution of tetrabutylammonium fluoride (11 mL) and then stirred for 1 h at room temperature. The reaction was quenched with H_2O and extracted with CH_2Cl_2 (3 × 50 mL). The combined organic extracts were dried over anhydrous Na_2SO_4 and concentrated using rotary evaporation. The resulting oil was purified by chromatography over silica gel eluting with hexane–ethyl acetate/triethylamine (5 : 1 : 0.01), affording compound **4** as a colourless oil (1.45 g, 98%). ^{1}H NMR (300 MHz, $CDCl_3$): δ = 7.43 (m, 2H), 7.26–7.34 (m, 6H), 7.19–7.24 (m, 1H), 6.83 (d, *J* = 8.9 Hz, 4H), 3.91 (m, 1H), 3.79 (s, 6H), 3.24 (m, 2H), 2.47 (ddd, *J* = 0.8, 2.6, 6.2 Hz, 2H), 2.37 (d, *J* = 5.0 Hz, 1H), 1.98 (t, *J* = 2.7 Hz, 1H). ^{13}C NMR (75 MHz, $CDCl_3$): δ = 158.71, 144.88, 136.06, 130.20, 128.28, 128.00, 127.01, 113.32, 86.43, 80.52, 70.67, 69.45, 66.06, 55.37, 24.07. IR (thin film): 3287, 3000, 2836, 2045, 1734, 1607, 1581, 1507, 1462, 1444, 1299, 1245, 1174, 1154, 1072, 1031, 951, 913, 826, 790, 772, 754, 701, 634, and 582 cm^{-1}. HRMS: *m*/*z* [M + Na]$^+$ calcd for $C_{26}H_{26}O_4Na_1$: 425.1723; found: 425.1723.

This journal is © The Royal Society of Chemistry 2011

Published on 02 March 2011 on http://pubs.rsc.org | doi:10.1039/C0OB00439A
Downloaded by Brown University on 05 January 2013

Compound 6. Compound **5**[27–29] (198 mg, 0.33 mmol), $Pd(PPh_3)_4$ (75.8 mg, 0.07 mmol) and CuI (25 mg, 0.13 mmol) were placed in a Schlenk flask and the flask was evacuated and recharged with N_2 gas. Dry THF (7 mL) and dry Et_3N (6 mL) were added and the resulting mixture was degassed for 10 min. Then compound **4** (263.8 mg, 0.66 mmol) in anhydrous THF (3 mL) was added and the mixture was stirred for 12 h at 65 °C. After cooling to room temperature, the mixture was poured into saturated aqueous $NaHCO_3$, extracted with CH_2Cl_2 (3 × 40 mL), dried over Na_2SO_4, filtered, and evaporated. The resulting residue was purified by chromatography over silica gel eluting with hexane–dichloromethane/triethylamine (1 : 1 : 0.01), affording compound **6** as a purple foam (289 mg, 95%). ^{1}H NMR (300 MHz, $CDCl_3$): δ = 10.05 (s, 1H), 9.41 (d, *J* = 4.6 Hz, 2H), 9.25 (d, *J* = 4.5 Hz, 2H), 8.96 (d, *J* = 4.5 Hz, 2H), 8.91 (d, *J* = 4.6 Hz, 2H), 8.19 (dd, *J* = 1.6, 7.5 Hz, 4H), 7.78 (m, 6H), 7.36 (m, 2H), 7.18–7.26 (m, 6H), 7.10–7.15 (m, 1H), 6.57 (dd, *J* = 1.3, 8.9 Hz, 4H), 3.74 (m, 1H), 3.38 (m, 1H), 3.33 (d, *J* = 2.0 Hz, 6H), 3.25 (m, 1H), 2.75 (m, 2H). ^{13}C NMR (125 MHz, $CDCl_3$): δ = 158.42, 152.08, 150.42, 149.77, 149.61, 144.99, 142.94, 135.89, 134.90, 132.54, 132.34, 131.78, 130.97, 130.11, 128.18, 128.00, 127.52, 126.93, 126.69, 120.97, 113.29, 107.06, 86.41, 69.92, 66.35, 55.07, 53.55, 29.85, 25.42. IR (thin film): 3052, 2933, 2831, 1597, 1506, 1489, 1459, 1439, 1382, 1298, 1245, 1219, 1173, 1153, 1058, 1031, 989, 904, 825, 790, 749, 727, 716, 619, 580 cm^{-1}. HRMS: *m/z* $[M + H]^+$ calcd for $C_{58}H_{45}N_4O_4Zn_1$: 925.2727; found: 925.2726.

Compound 1. To a solution of compound **6** (93.6 mg, 0.10 mmol) and *N*,*N*-diisopropylethylamine (0.1 mL, 0.54 mmol) in anhydrous CH_2Cl_2 (4 mL) was added 2-cyanoethyl *N*,*N*-diisopropylchlorophosphoramidite (0.034 mL, 0.15 mmol). After 2 h, the reaction mixture was poured into saturated aqueous $NaHCO_3$ and extracted by CH_2Cl_2 (3 × 40 mL). The organic layer was evaporated to dryness and the resulting residue was purified by chromatography over silica gel eluting with hexane–dichloromethane/triethylamine (2 : 1 : 0.01), affording compound **1** as a purple foam (85 mg, 74%). (Compound **1** is a mixture of two diastermers, the ratio of major and minor isomers is around 2 : 1 according to ^{1}H NMR.) ^{1}H NMR (500 MHz, $CDCl_3$): δ = 10.04 (s, 2H), 9.64 (d, *J* = 4.5 Hz, 2H), 9.59 (d, *J* = 4.6 Hz, 2H), 9.23 (d, *J* = 4.5 Hz, 4H), 8.93–3.98 (m, 8H), 8.23 (d, *J* = 7.3 Hz, 8H), 7.77–7.83 (m, 12H), 7.51–7.56 (m, 4H), 7.30–7.38(m, 8H), 7.19–7.25 (m, 4H), 7.09–7.14 (m, 2H), 6.50 (d, *J* = 8.9 Hz, 2H), 6.47 (d, *J* = 8.9 Hz, 2H), 6.40 (d, *J* = 8.9 Hz, 2H) (minor isomer), 6.32 (d, *J* = 8.8 Hz, 2H) (minor isomer), 4.57–4.69 (m, 2H), 3.63–3.98 (m, 12H), 3.55–3.60 (m, 2H), 3.38–3.46 (m, 2H), 3.23 (s, 3H), 3.18 (s, 3H), 3.08 (s, 3H) (minor isomer), 2.97 (s, 3H) (minor isomer), 2.41–2.60 (m, 2H), 2.31–2.37 (m, 2H) (minor isomer), 1.32 (d, *J* = 6.8 Hz, 6H) (minor isomer), 1.25 (d, *J* = 6.8 Hz, 6H) (minor isomer), 1.20 (d, *J* = 6.8 Hz, 6H), 1.17 (d, *J* = 6.8 Hz, 6H). ^{13}C NMR (125 MHz, $CDCl_3$): δ = 158.22, 158.13, 158.10, 157.94, 152.20, 152.15, 150.43, 150.41, 149.83, 149.70, 149.67, 145.35, 145.32, 142.76, 136.38, 136.29, 136.04, 136.00, 134.72, 132.55, 132.50, 131.85, 131.30, 130.32, 130.13, 130.06, 128.32, 128.28, 127.90, 127.85, 127.62, 126.77, 121.10, 117.80, 117.63, 113.20, 113.17, 113.14, 113.11, 106.98, 86.35, 86.30, 73.12, 72.97, 72.33, 72.20, 65.95, 65.94, 65.79, 65.78, 58.78, 58.74, 58.64, 58.60, 55.10, 54.96, 54.92, 54.84, 43.64, 43.54, 43.49, 25.89, 25.84, 25.81, 24.91, 24.56, 24.81, 24.76, 20.48, 20.42, 20.41, 20.36. ^{31}P NMR (121 MHz, $CDCl_3$): δ = 148.05, 147.85. IR (thin film): 2962, 2930, 2866, 2834, 2253, 2227, 2022, 1507, 1490, 1460, 1440, 1382, 1363, 1297, 1248, 1176, 1154, 1124, 1060, 1032, 1002, 992, 908, 827, 792, 780, 751, 728, 717, 700, 658, 582 cm^{-1}. HRMS: *m/z* $[M + H]^+$ calcd for $C_{67}H_{62}N_6O_5P_1Zn_1$: 1125.3805; found: 1125.3807.

GNA oligonucleotide synthesis and purification

General protocol[30]. All oligonucleotides were prepared on an ABI 394 DNA/RNA synthesizer on a 1 μmole scale. A standard protocol for 2-cyanoethyl phosphoramidites (0.1 M) was used, except that the coupling time was extended to 3 min for A and T nucleotides and 15 min for porphyrin phosphoramidite couplings. After the trityl-on synthesis, the resin was incubated with conc. aq. NH_3 solution (1.5 mL) for 12 h at 55 °C. After cooling, the entire solution was applied directly to a Sep–Pak Classic reversed-phase column (Waters, 360 mg) and washed sequentially with 3% NH_4OH (15 mL), water (10 mL), 1.5% aqueous TFA (10 mL), and finally water (10 mL). The oligo was then eluted with 20% aqueous acetonitrile or 30% for oligonucleotides containing porphyrins and further purified using a Waters XTerra column (MS C18, 4.6 × 50 mm, 2.5 μm) at 55 °C with aqueous TEAA and acetonitrile as the eluent. The identities of all oligonucleotides were confirmed by MALDI-TOF MS.

Zinc metallation of porphyrin in GNA. To a solution of porphyrin-GNA single strands (12 nmol GNA single strands in 140 μL of 10 mM Tris-HCl buffer solution, pH 7.6) was added a solution of $Zn(OAc)_2$ in H_2O (10 mM, 12 μL,10 eq.). The solution was shaken at 25 °C and the reaction was followed by absorption spectroscopy. After around 2 h, the reaction mixture was diluted to 1000 μL with 3% ammonia solution. Excess Zn^{2+} was removed by treating the reaction mixture with ion-exchange resins (Chelex 100 sodium form). The strands were purified by HPLC using a Water XTerra column at 55 °C with aqueous TEAA and acetonitrile as the eluent. The identities of the oligonucleotides was confirmed by MALDI-TOF MS.

Nickel metallation of porphyrin in GNA. Nickel metallation was carried out by heating (80 °C) under nitrogen atomosphere a solution of porphyrin-GNA single strands (2.5 nmol GNA in 325 μL of 10 mM Tris-HCl buffer solution, pH 7.6, and 10 mM $Ni(OAc)_2$). The reaction was followed by absorption spectroscopy and found to be completed after heating for 16 h. Workup was performed in analogy to the zinc(II) complexation.

Analysis of GNA nucleic acids

Thermal denaturation. The melting studies were carried out in 1 cm path length quartz cells (total volumn 325 μL; 200 μL sample solutions were covered by mineral oil) on a Beckman 800 UV-Vis spectrophotometer equipped with a thermo-programmer. Melting curves were monitored at 260 nm with a heating rate of 1 °C min^{-1}. Melting temperatures were calculated from the first derivatives of the heating curves. Experiments were performed in duplicate and mean values were taken.

UV-vis spectroscopy. The absorptions of oligonucleotide solutions were measured in a quartz cuvette with a path length of 1 cm at 260 nm on Beckman 800 UV-Vis spectrophotometer. Temperature-dependent absorption spectra were obtained

View Article Online

on Beckman 800 UV-Vis spectrophotometer equipped with a temperature controller. Spectra were obtained every 10 °C by heating from 20 to 80 °C. Both single strands and duplexes (2 μM of each strand) were prepared in 10 mM sodium phosphate, 100 mM NaCl, pH 7.0.

Fluorescence spectroscopy. The experiments were performed in 96-well plates on a Molecular Devices SpectraMax M5 with excitation at 427 nm and a cutoff filter at 435 nm. The experiments with single strands or duplexes were performed in 10 mM sodium phosphate, 100 mM NaCl, pH 7.0, and the concentration of each strand was 2 μM.

CD spectroscopy. CD measurements were performed on a JASCO J-810 spectrometer in a 1 mm path length quartz cuvette. The GNA single strands or duplexes were prepared in 10 mM sodium phosphate, 100 mM NaCl, pH 7.0, and the concentration of each strand was 12 μM. Each measurement was repeated 5 times and the average taken.

Computational work

Models of **ON6**:**ON7** and **ON10**:**ON11** were built based on a previously described GNA model.[26] In short, crystal structure of an 8mer duplex of a GNA analog[26] was extended by including an additional end-to-end stacked duplex from the crystal lattice using the Pymol program[31] and refined using MD simulations. In order to create the models for the porphyrin containing GNA, the nucleobases from the parent GNA were removed leaving only the nitrogen linkage to the backbone and the flanking carbons. This allows the plane of the nucleobase to be properly defined and the *xleap* module of AMBER[32] was used to add the remaining atoms. As the porphyrin moiety is incorporated through an acetylene linkage, the proper definition of the plane is not possible and the porphyrin residues must be manually rotated into the GNA duplex. Charges for all residues were assigned by RESP fitting on HF/6-31-G* optimized structures. Intermolecular charge constraints were used to ensure equivalent charges along the backbone, which were neutralized by adding 30 Na^+ ions using *xleap*. The solute was placed into a pre-equilibrated box of TIP3P water extending 10 Å beyond the solute in all directions. The initial models were minimized first by restraining solute atoms while relaxing the sodium ions and solvent, followed by minimization using constraints to fix the base pair hydrogen bonds and to position the porphyrin moieties properly within the duplex. Finally, an unrestrained minimization was performed in preparation for MD. The Particle Mesh Ewald Molecular Dynamics (*pmemd*) module of AMBER was used to perform all MD simulations to improve the efficiency of the parallel simulations. Force field parameters for the simulations were adopted from the Cornell *et al.* forcefield, along with the adjustments by Wang *et al.* (parm99).[33,34] Parameters for unmodified GNA bases and glycol backbone were taken directly from the Cornell *et al.* force field. Heating of the system from 0–300° K was performed in the NVT ensemble over 20 ps with restraints on the solute. From there, equilibration and production runs were performed in the NPT ensemble resulting in 50 ns trajectories for both sequences studied. The *ptraj* module of AMBER was used for all post-processing of the trajectory data.

Published on 02 March 2011 on http://pubs.rsc.org | doi:10.1039/C0OB00439A
Downloaded by Brown University on 05 January 2013

Acknowledgements

We thank the Philipps-University Marburg for financial support.

Notes and references

1 E. Schwartz, S. Le Gac, J. J. L. M. Cornelissen, R. J. M. Nolte and A. E. Rowan, *Chem. Soc. Rev.*, 2010, **39**, 1576.
2 F. J. M. Hoeben, P. Jonkheijm, E. W. Meijer and A. P. H. J. Schenning, *Chem. Rev.*, 2005, **105**, 1491.
3 V. Palermo, E. Schwartz, C. E. Finlayson, A. Liscio, M. B. J. Otten, S. Trapani, K. Müllen, D. Beljonne, R. H. Friend, R. J. M. Nolte, A. E. Rowan and P. Samori, *Adv. Mater.*, 2010, **22**, E81.
4 (*a*) M. R. Wasielewski, *Acc. Chem. Res.*, 2009, **42**(12), 1910; (*b*) D. Astruc, E. Boisselier and C. Ornelas, *Chem. Rev.*, 2010, **110**, 1857; (*c*) A. P. H. J. Schenning and E. W. Meijer, *Chem. Commun.*, 2005, 3245.
5 (*a*) E. M.-Enthart, C. Wagner, J. Barbaric and H.-A. Wagenknecht, *Tetrahedron*, 2007, **63**, 3434; (*b*) H.-A. Wagenknecht, *Angew. Chem., Int. Ed.*, 2009, **48**, 2838; (*c*) R. Varghese and H.-A. Wagenknecht, *Chem. Commun.*, 2009, 2615; (*d*) J. Gao, S. Watanabe and E. T. Kool, *J. Am. Chem. Soc.*, 2004, **126**, 12748.
6 V. L. Malinovskii, D. Wenger and R. Häner, *Chem. Soc. Rev.*, 2010, **39**, 410.
7 K. C. Hannah and B. A. Armitage, *Acc. Chem. Res.*, 2004, **37**, 845.
8 (*a*) M.-S. Choi, T. Yamazaki, I. Yamazaki and T. Aida, *Angew. Chem., Int. Ed.*, 2004, **43**, 150; (*b*) D. Kim and A. Osuka, *Acc. Chem. Res.*, 2004, **37**, 735; (*c*) T. S. Balaban, *Acc. Chem. Res.*, 2005, **38**, 612; (*d*) M. Endo, M. Fujitsuka and T. Majima, *Chem.–Eur. J.*, 2007, **13**, 8660.
9 (*a*) L.-A. Fendt, I. Bouamaied, S. Thöni, N. Amiot and E. Stulz, *J. Am. Chem. Soc.*, 2007, **129**, 15319; (*b*) I. Bouamaied, T. N. Nguyen, T. Rühl and E. Stulz, *Org. Biomol. Chem.*, 2008, **6**, 3888; (*c*) T. N. Nguyen, A. Brewer and E. Stulz, *Angew. Chem., Int. Ed.*, 2009, **48**, 1974–1977.
10 M. Endo, M. Fujitsuka and T. Majima, *Tetrahedron*, 2008, **64**, 1839–1846.
11 S. Sitaula and S. M. Reed, *Bioorg. Med. Chem. Lett.*, 2008, **18**, 850–855.
12 (*a*) M. Endo, M. Fujitsuka and T. Majima, *J. Org. Chem.*, 2008, **73**, 1106; (*b*) M. Endo, T. Shiroyama, M. Fujitsuka and T. Majima, *J. Org. Chem.*, 2005, **70**, 7468; (*c*) M. Endo, N. C. Seeman and T. Majima, *Angew. Chem., Int. Ed.*, 2005, **44**, 6074.
13 (*a*) H. M.-Rojas and E. T. Kool, *Org. Lett.*, 2002, **4**, 4377; (*b*) T. Murashima, K. Hayata, Y. Saiki, J. Matsui, D. Miyoshi, T. Yamada, T. Miyazawa and N. Sugimoto, *Tetrahedron Lett.*, 2007, **48**, 8514; (*c*) K. Berlin, R. K. Jain, M. D. Simon and C. Richert, *J. Org. Chem.*, 1998, **63**, 1527.
14 H. Zhou, X. Ma, J. Wang and L. Zhang, *Org. Biomol. Chem.*, 2009, **7**, 2297.
15 L. Zhang, A. Peritz and E. Meggers, *J. Am. Chem. Soc*, 2005, **127**, 4171.
16 M. K. Schlegel, L.-O. Essen and E. Meggers, *J. Am. Chem. Soc.*, 2008, **130**, 8158.
17 E. Meggers and L. Zhang, *Acc. Chem. Res.*, 2010, **43**, 1092.
18 M. K. Schlegel, L.-O. Essen and E. Meggers, *Chem. Commun.*, 2010, **46**, 1094.
19 R. F. Pasternack, L. Francescon, D. Raff and E. Spiro, *Inorg. Chem.*, 1973, **12**, 2606.
20 W. Zhen, N. Shan, L. Yu and X. Wang, *Dyes Pigm.*, 2007, **77**, 153.
21 (*a*) Y. Kobuke and H. Miyaji, *J. Am. Chem. Soc.*, 1994, **116**, 4111; (*b*) F. Hajjaj, Z. S. Yoon, M.-C. Yoon, J. Park, A. Satake, D. Kim and Y. Kobuke, *J. Am. Chem. Soc.*, 2006, **128**, 4612; (*c*) K. Ogawa, T. Zhang, K. Yoshihara and Y. Kobuke, *J. Am. Chem. Soc.*, 2002, **124**, 22.
22 (*a*) M. Shirakawa, S.-I. Kawano, N. Fujita, K. Sada and S. Shinkai, *J. Org. Chem.*, 2003, **68**, 5037; (*b*) N. C. Maiti, S. Mazumdar and N. Periasamy, *J. Porphyrins Phthalocyanines*, 1998, **2**, 369.
23 D. R. McMillin, A. H. Shelton, S. A. Bejune, P. E. Fanwick and R. K. Wall, *Coord. Chem. Rev.*, 2005, **249**(13–14), 1451.
24 Y. Nitta and R. Kuroda, *Biopolymers*, 2006, **81**, 376.
25 (*a*) A. Mammana, T. Asakawa, K. B.-Jensen, A. Wolfe, S. Chaturantabut, Y. Otani, X. Li, Z. Li, K. Nakanishi, M. Balaz, G. A. Ellestad and N. Berova, *Bioorg. Med. Chem.*, 2008, **16**, 6544; (*b*) M. Balaz, K. B.-Jensen, A. Mammana, G. A. Ellestad, K. Nakanishi and N. Berova, *Pure Appl. Chem.*, 2007, **79**, 801.
26 A. T. Johnson, M. K. Schlegel, E. Meggers, L.-O. Essen, O. Wiest, to be published.

 This journal is © The Royal Society of Chemistry 2011

View Article Online

27 V. S.-Y. Lin, P. M. Iovine, S. G. Dimango and M. J. Therien, *Inorg. Syn.*, 2002, **33**, 55.
28 (*a*) M. Fazekas, M. Pintea, M. O. Senge and M. Zawadzka, *Tetrahedron Lett.*, 2008, **49**(14), 2236; (*b*) T. S. Balaban, R. Goddard, M. L.-Schaetzel and J.-M. Lehn, *J. Am. Chem. Soc.*, 2003, **125**, 4233.
29 H. Kai, S. Nara, K. Kinbara and T. Aida, *J. Am. Chem. Soc.*, 2008, **130**, 6725.
30 L. Zhang, A. E. Peritz, P. J. Carroll and E. Meggers, *Synthesis*, 2006, 645.
31 W. L. DeLano The, PyMOL Molecular Graphics System, 2002, DeLano Scientific, San Carlos, CA, USA.
32 D. A. Case, T. E. Cheatham III, C. L. Simmerling, J. Wang, R. E. Duke, R. Luo, M. Crowley, W. Zhang, K. M. Merz, B. Wang, S. Hayik, A. Roitberg, G. Seabra, I. Kolossváry, F. Paesani, J. Vanicek, X. Wu, S. R. Brozell, T. Steinbrecher, H. Gohlke, L. Yang, J. Mongan, V. Hornak, G. Cui, D. H. Mathews, M. G. Seetin, C. Sagui, V. Babin, P. A. Kollman, *AMBER10*, 2008, University of California, San Francisco.
33 W. D. Cornell, P. Cieplak, C. I. Bayly, I. R. Gould, K. M. Merz, D. M. Ferguson, D. C. Spellmeyer, T. Fox, J. W. Caldwell and P. A. Kollman, *J. Am. Chem. Soc.*, 1995, **117**, 5179.
34 J. M. Wang, P. Cieplak and P. A. Kollman, *J. Comp. Chem.*, 2000, **21**, 1049.

Published on 02 March 2011 on http://pubs.rsc.org | doi:10.1039/C0OB00439A
Downloaded by Brown University on 05 January 2013